NJC

ROYAL SOCIETY OF CHEMISTRY

PAPER

View Article Online
View Journal

Cite this: DOI: 10.1039/d6nj01284a

Electron deficient confined spaces within naphthalene diimide cryptophanes

Élise Antonetti,[a] Sabine Michaud-Chevallier,[a] Marion Jean,[b] Muriel Serradeil-Albalat,[b] Nicolas Vanthuyne,[b] Paola Nava,*[a] Alexandre Martinez*[a] and Yoann Cotelle*[a]

Received 7th April 2026,
Accepted 18th May 2026

DOI: 10.1039/d6nj01284a

rsc.li/njc

In order to enhance the recognition properties of a given substrate, to increase the stability of an intermediate or to sequester a pollutant from its medium, the development of suitable confined spaces is an attractive strategy. However, most of the covalent cages described in the literature are based on electron rich scaffolds, thus limiting access to electron deficient confined spaces. Naphthalene diimides are broadly used as π-acidic surfaces and can additionally serve as recognition units through anion–π interactions thanks to their high quadrupole moments. In order to preorganize the naphthalene diimide units into a well-defined confined space, cryptophanes are well-suited because of the rigidity of the cyclotriveratrylene moieties, their bowl shape and their well-known synthesis. Herein, we describe the synthesis of two diastereoisomers of a cryptophane having three naphthalene diimide spacers, their characterization, the resolution of the racemate and their recognition properties towards selected anions and pyrene.

Introduction

The synthesis of covalent molecular cages, delimiting an accessible three dimensional void cavity, has occupied synthetic and supramolecular chemists for more than fifty years, in order to mimic the well-defined enzyme binding vestibules.[1–4] Thus, this area of research enabled the discovery of molecular containers, including cryptands,[5] cavitands,[6] cryptophanes[7] and hemicryptophanes,[8] for the encapsulation of naturally occurring compounds,[9,10] as well as abiotic ones[11,12] through non-covalent interactions[13] and/or confinement effects.[14] However, the introduction of endohedral functional units with a precise design still remains difficult.[15–17] The synthetic limitations for covalent cages also hampered the introduction of emerging interactions such as the anion–π interaction.[18] Nonetheless, this electrostatic interaction between an anion and an electron deficient aromatic surface, having a strong positive quadrupole moment, offers new opportunities for selectivity in both molecular recognition and catalysis thanks to its peculiar binding mode.[19–22] Among the electron deficient surfaces known to bind anions through anion–π interactions, naphthalene diimides (NDIs) possess one of the strongest quadrupole moments (Q_{ZZ} = 13.7 B, at the MP2/aug-cc-pVTZ computational level)[23] and their functionalization on the imide position is well documented and amenable over a large range of substrates. NDIs have been used for the construction of molecular cages;[24–30] however, anion–π interactions were not described for neutral NDI-covalent cages.[31–34] Recently, we described a molecular cage having three NDI walls linked by two benzene triimide units able to bind anions, and having an unexpected hourglass conformation.[35] In order to obtain a well-defined electron deficient confined space to expand the applications of anion–π interactions, cryptophanes appear as suitable preorganized scaffolds.[36] Indeed, the presence of two cyclotriveratrylene (CTV) units should prevent the electron deficient aromatic surface aggregation while maintaining a well-defined cavity delimited by the two CTVs and the three π-acidic surfaces (Fig. 1). Hereby, we describe the synthesis of a cryptophane receptor containing three naphthalene diimide spacers, its characterization, chiroptical properties and its binding ability towards anions through anion–π interactions as well as towards pyrene.

Results and discussion

Cryptophanes can be synthesized through three different strategies:[7] (1) the direct method which consists of the trimerization of bis(vanillyl alcohol) precursors linked through a spacer. This method proved to be easy and fast to perform; however, both the yields and the *anti*/*syn* ratio strongly depend on the

[a] Aix Marseille Univ, CNRS, Centrale Med, ISM2, Marseille, France. E-mail: paola.nava@univ-amu.fr, alexandre.martinez@centrale-marseille.fr, yoann.cotelle@univ-amu.fr
[b] Aix Marseille Univ, CNRS, Centrale Med, FSCM, Chiropole, Marseille, France

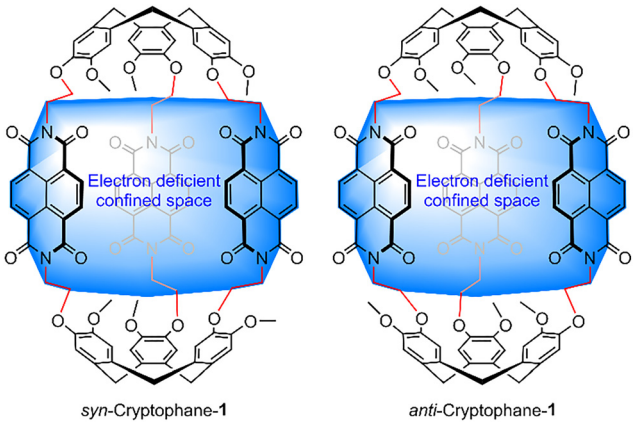

Fig. 1 Schematization of the electron deficient confined space within NDI-cryptophane **1**.

nature of the linkers between the bis(vanillyl alcohol) units. (2) The coupling method is done by reacting two CTVs with the linkers in a one pot sequence. It gives comparable yields to the direct method and is equally straightforward. (3) Finally, the template method can be realized by grafting three vanillyl alcohol substituents onto a CTV molecule. This method gives the highest yields but necessitates more intensive synthetic sequences.

As a starting point, NDI cryptophanes were synthesized using the direct method. A short synthesis was developed to afford naphthalene diimide precursor **5**, bearing two protected vanillyl alcohol substituents, in three steps with 33% yield and without any column chromatography purification (Scheme 1). The Gabriel synthesis was applied to THP protected bromoethoxyvanillyl alcohol **2** to obtain THP protected vanillylalcoholethanamine **4**. A nucleophilic substitution was performed on compound **2** using potassium phthalimide in DMF, followed by the deprotection of amine using hydrazine in MeOH. The last step consisted of the condensation of two equivalents of the free amine on naphthalene dianhydride in the presence of DIPEA in DMF by heating at 130 °C for 16 h. After the reaction,

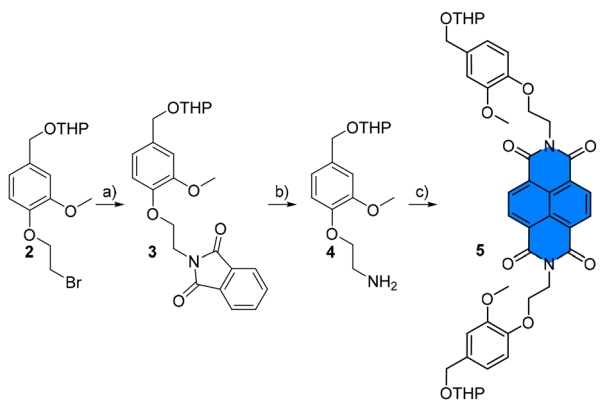

Scheme 1 Synthesis of precursor **5**. (a) Potassium phthalimide, DMF, 85 °C, 2 h, and 63%. (b) Hydrazine, MeOH, 80 °C, 3 h, and 65%. (c) Naphthalene dianhydride **6**, DIPEA, DMF, 130 °C, 16 h, and 80%.

NDI precursor **5** was simply obtained by precipitation in water with 80% yield.

Next, the cyclization reaction was performed at room temperature in formic acid at 1.0 mM (Scheme 2). After ten days of reaction, we were pleased to observe the desired product in the reaction mixture. After multiple purification procedures (see below), we were finally able to obtain *syn*-cryptophane **1** and *anti*-cryptophane **1** in a 1 : 1 ratio with a combined yield of 2.5%. The reaction conditions were then optimized, starting from the precipitation of NDI precursor **5**. In fact, precursor **5** was first obtained by precipitation in aqueous HCl 1 M solution, which was obviously replaced by water. Although the yield for the obtention of compound **5** was greatly improved, the cyclization in formic acid did not afford any traces of cryptophane **1** (Table 1, entry 2). Consequently, we started adding controlled HCl equivalents from concentrated aqueous HCl solutions. By adding one equivalent of HCl, we were pleased to obtain up to 4.2% yield of cryptophane **1** (Table 1, entry 3). Adding more equivalents of HCl, from twelve to fifty, did not improve the outcome of the reaction, and decreased the yields until no trace of the product could be observed (Table 1, entries 4–6). Since our receptors are built to operate with anion–π interactions, we decided to try another source of chloride anions, and chose to use tetrabutylammonium (TBA) chloride. This reaction gave cryptophane **1** with a 2.7% yield. While the yield is decreasing compared to the use of HCl, it indicates that the presence of chloride anions is needed for the obtention of our receptor as no product is obtained under the same conditions without this salt. Finally, the temperature of the reaction was slightly increased to 40 °C; however, this did not increase the yield either (Table 1, entry 8). The optimization of the reaction conditions indicates a clear beneficial impact of chloride anions to obtain cryptophane **1**; at this stage, we putatively impute this effect arising from a templated effect of the chloride anions. The obtention of NDI cryptophane **1** by the direct method was successful; however, the modest yield of 4.2% led to the investigation of other synthetic pathways. Next, the coupling method was performed between two equivalents of CTV-NH_2 **7**[37] and three equivalents of naphthalene dianhydride **6** (Scheme 2). The reaction was first performed using DIPEA in DMF at 130 °C for 16 h and did not give any trace of the product but instead oligomers were observed in the ^{1}H NMR of the crude. Then, the reaction was performed under microwave irradiation in DMF for 30 min and gave a combined yield of 1.5%; thus, this second pathway did not improve our total yield. Finally, the template method was initiated starting from CTV-NH_2 **7**, NDA **6** and vanillyl alcohol (results not shown); unfortunately, the cyclization precursor of cryptophane **1** proved to be insoluble and thus we decided not to follow this pathway.

The purification of the crude mixture was performed by successive silica gel column chromatography followed by size exclusion chromatography and finally semi-preparative chiral stationary phase HPLC (see the SI). We were pleased to find conditions that allow separation of all diastereoisomers (*syn*-**1** and *anti*-**1**) and enantiomers (*anti*-(*PP*) and *anti*-(*MM*)). For this,

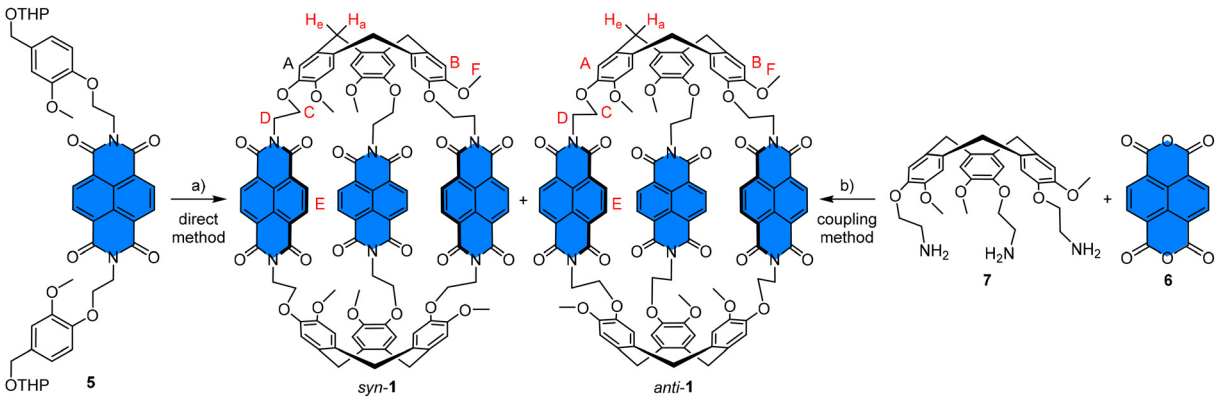

Scheme 2 Synthesis of cryptophane **1** giving a 1 : 1 mixture of *syn* and *anti*-diastereoisomers using the (a) direct method: 1.0 mM, formic acid, HCl (1 equiv.) 25 °C, 10 days, and 4.2% and (b) coupling method: 2.0 mM, DMF, 0.5 h, 45 °C then 130 °C, and 1.5%.

Table 1 Optimization of the conditions for the obtention of cryptophane **1**

Entry	T (°C)	Additives[a]	Yield (%)
1	25	HCl (traces)[b]	2.5
2	25	None	Not observed
3	25	HCl (1 equiv.)	4.2
4	25	HCl (12 equiv.)[c]	3.4
5	25	HCl (25 equiv.)	1.3
6	25	HCl (50 equiv.)	Not observed
7	25	TBACl (1 equiv.)	2.7
8	40	HCl (1 equiv.)	2.1

[a] General conditions: formic acid, 1.0 mM, 25 °C, and 10 days. The equivalents of the additives are calculated towards precursor **5**. [b] Traces of HCl obtained from the precipitation of precursor **2**. [c] Added after 12 days.

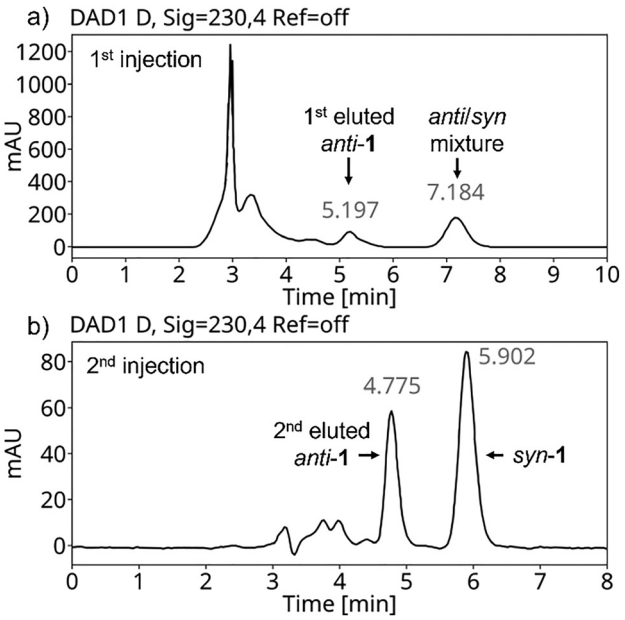

Fig. 2 Chiral stationary phase HPLC chromatograms of cryptophane **1**: (a) Chiralpak IB N-5, DCM/EtOH 60 : 40, and 1 mL min^{-1} and (b) Chiral art cellulose SJ, DCM/EtOH 50 : 50, and 1 mL min^{-1}.

a first injection was performed on a chiralpak IB N-5 column using a DCM/EtOH mixture (3 : 2) as the eluent. A first eluted fraction was obtained at 5.2 min and corresponds to one enantiomer of *anti*-cryptophane **1** (Fig. 2a). The second elution peak at 7.2 min corresponds to a mixture of the second enantiomer of *anti*-cryptophane **1** and achiral *syn*-diastereoisomer **1**. After the screening of several chiral stationary phases, we managed to separate the second enantiomer of *anti*-cryptophane **1** at 4.8 min and *syn*-cryptophane **1** at 5.9 min using a chiral art cellulose SJ stationary phase using a DCM/EtOH solvent mixture (1 : 1) (Fig. 2b). A 1 : 1 diastereomeric ratio between *syn* and *anti* diastereoisomers was obtained for the direct method coupling, which usually tends to favor the *anti* diastereoisomer.[7]

syn-Cryptophane **1** and *anti*-cryptophane **1** were fully characterized by ^{1}H, ^{13}C, and MS techniques (Fig. S8–S11). The ^{1}H NMR spectrum of *syn*-cryptophane **1** reflects its average C_{3h} symmetry notably by the presence of a doublet at 3.48 ppm for H_e protons, a singlet at 3.72 ppm for protons F, and two singlets for the aromatic protons at 6.76 and 6.87 ppm for protons A and B, respectively (Fig. 3a). The aromatic NDI protons E are also well resolved and appear as a singlet at 8.59 ppm. The aliphatic protons C and D coming from the linker between the CTV, the NDI and the H_a protons are observed as three multiplets between 4.2 and 4.7 ppm. The ^{1}H NMR spectrum of *anti*-cryptophane **1** closely resembles that of *syn*-cryptophane **1** (Fig. 3b). The H_e protons can be observed as a doublet at 3.47 ppm. The singlet at 3.69 ppm corresponds to the protons F. Protons H_a, C and D appear as three multiplets between 4.25 ppm and 4.68 ppm. The aromatic protons A, B and E resonate at 6.74 ppm, 6.83 ppm and 8.60 ppm, respectively, as three singlets.

Unfortunately, single crystals of cryptophane **1** could not be grown from crystallization experiments using multiple solvents and combinations of solvents. Nevertheless, a structure for each electron deficient cage could be optimized using DFT calculations (PBE0-D3/def2-TZVP). The geometry optimization was performed by imposing a C_3 symmetry axis, in accordance with the ^{1}H NMR spectra in solution (Fig. 4a and b). The *syn*

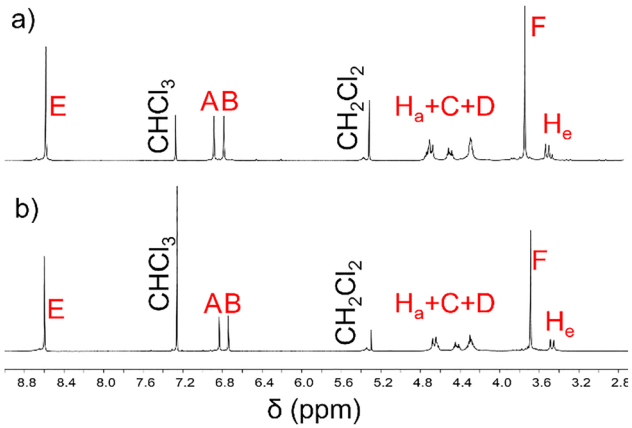

Fig. 3 (a) ^{1}H NMR spectra of *syn*-cryptophane **1** ($CDCl_3$, 298 K, and 400 MHz). (b) ^{1}H NMR spectra of *anti*-cryptophane **1** ($CDCl_3$, 298 K, and 400 MHz).

and *anti*-isomers possess two distinctive conformations, and the s*yn*-cage has a very large cavity, delimited by the two CTVs and the three NDI arms, with a volume of 767 Å^3. The *anti*-isomer presents an interesting conformation showing a helical arrangement of the NDI arms and a much smaller cavity with a volume of 391 Å^3. Moreover, no stacking between the NDI units is observed, which validates our strategy of using the CTV as a preorganizing unit to prevent intramolecular self-assembly of the aromatic units. Interestingly, the ECD spectra recorded for the two enantiomers of *anti*-cryptophane **1** bring some information about their conformations. First, the two ECD spectra show mirror images confirming their enantiomeric nature. Secondly, the presence of an ECD signal at 360 and 380 nm, which corresponds to the absorption of NDI units, shows the chirality induction from the chiral CTV units to the NDIs (Fig. 4c and d). Finally, no excitonic coupling for the NDI signals is observed. Taken together, these elements confirm the helicity determined by DFT calculations.

Once the two diastereomers were isolated and characterized, their recognition properties towards anions through anion–π interactions were investigated. Titrations were performed in DCM at constant host concentrations and were followed by UV-visible spectroscopy. The TBA salts were chosen in order to avoid inclusion of the cation during titration experiments. The binding experiments revealed efficient binding of iodide, nitrate and tetrafluoroborate with a 1 : 1 stoichiometry for both *syn* and *anti*-cryptophane **1** from K_a = 10 000 ± 4% (I-@*syn*-**1**) to K_a = 32 000 ± 3% (NO_3^-@*syn*-**1**). However, only moderate selectivity between the two diastereoisomers could be observed (Fig. 5a). The high binding affinities for anions support our strategy of combining several electron deficient surfaces within a confined space to favor anion recognition. The structure of NO_3^-@*anti*-**1** was optimized at the DFT level, revealing an arrangement of the anion in the cage that is compatible with anion–π interactions (Fig. S31). Finally, in order to gain insights into the role of chloride during the synthesis of cryptophane, we performed titrations of cryptophane **1** with aliquots of a chloride solution. No significant binding could be determined by UV-visible titrations thus excluding the template effect of chloride during the final cyclization. However, it could be possible that chloride acts as a template for the formation of dimers prior to the final cyclotrimerization. Anion recognition failed to demonstrate the differences of the two diastereoisomers' conformations indicated by the DFT optimized structures. For this purpose, pyrene was chosen as an additional guest because of its ability to generate charge transfer absorption bands in the presence of NDI receptors.[38,39] Titrations were also performed with constant host concentrations and were followed by UV-visible spectroscopy. For *syn*-cryptophane **1**, the appearance of an absorption band upon titration with pyrene

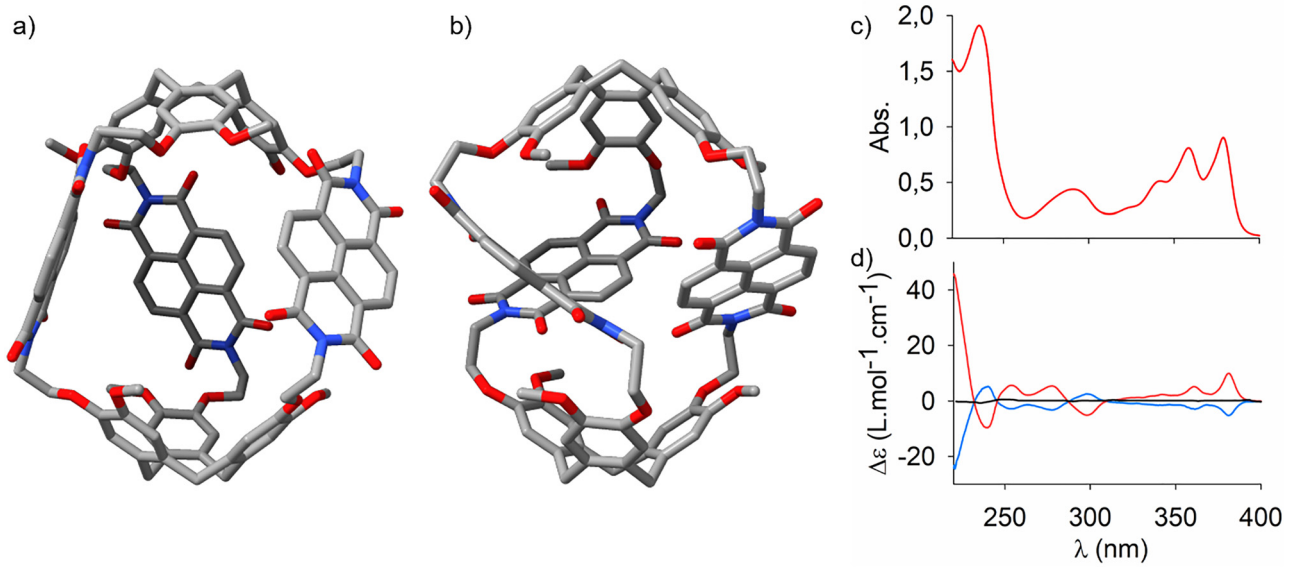

Fig. 4 Optimized DFT structures of (a) *syn* and (b) *anti*-cryptophane **1** (PBE0-D3/def2-TZVP). (c) UV spectra recorded for *anti*-cryptophane **1**. (d) ECD spectra recorded for *anti*-cryptophane **1** (first eluted, blue line; second eluted red line) and *syn*-cryptophane **1** (black line) in DCM.

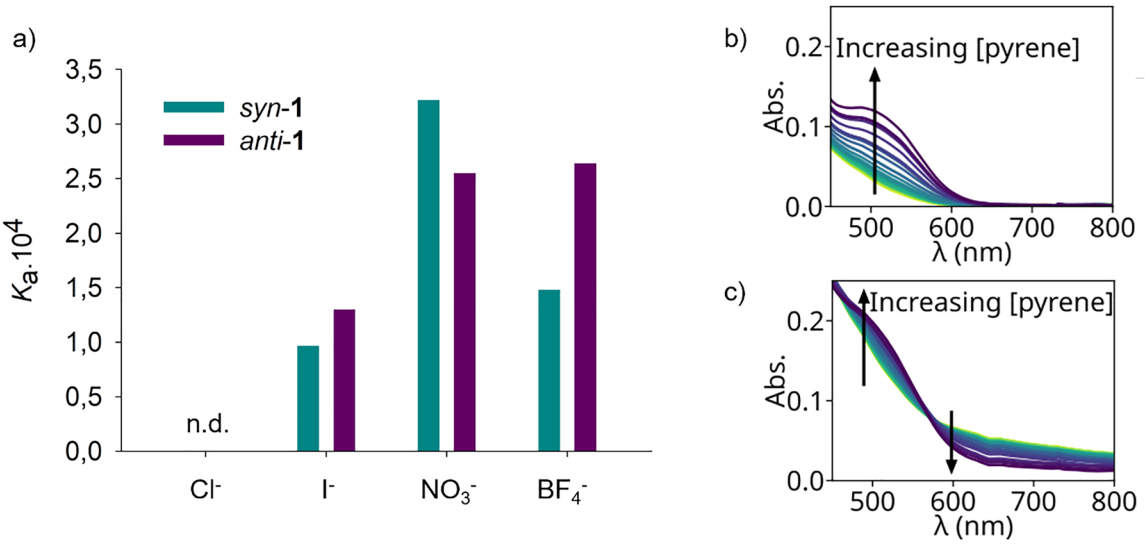

Fig. 5 (a) Binding constants between anions and *syn* or *anti*-isomers of cryptophane **1** in DCM determined by UV-visible titrations. (b and c) Titration experiments of cryptophane: (b) *syn*-cryptophane **1** (5×10^{-4} M) and (c) *anti*-cryptophane 5×10^{-4} M **1** by pyrene (5×10^{-2} M) at constant host concentrations in DCM. Arrows show the variation of absorbance upon titration.

between 450 nm and 650 nm is characteristic of a charge transfer; however, the binding constant is very low $K_a = 11 \pm 2\%$ (Fig. 5b). The observation of the charge transfer with a very low binding constant could be due to the large cavity volume of *syn*-cryptophane **1**. On the other hand, the titration of *anti*-cryptophane **1** by pyrene gives a different profile, with a weaker charge transfer absorption band between 450 nm and 550 nm together with an isosbestic point at 570 nm which clearly demonstrates the equilibrium between the bound and unbound pyrene (Fig. 5c). The binding constant here is $K_a = 91 \pm 4\%$ for a 1 : 1 stoichiometry. Thus, pyrene shows two different binding profiles towards *syn* and *anti*-cryptophanes **1**, which indicates that two different binding cavities are present.

Conclusions

This work aimed at developing an electron deficient cavity by developing NDI-cryptophanes for the recognition of anions. Through tedious synthesis and purification, we finally managed to synthesize and isolate the two diastereoisomers of cryptophane **1**. DFT optimization coupled with ^{1}H NMR and ECD spectra gave valuable insights into the conformations of these two covalent cages. While the *syn* cryptophane exhibits a large cavity, *anti*-cryptophane **1** shows a helical arrangement of the NDI units originating from an induced chirality from the CTV units. In order to differentiate the two hosts, pyrene titrations were performed, which showed two distinct behaviors. Finally, anion titrations display high binding constants between the cage receptors and the guests as a result of anion–π interactions. NDI-cryptophanes appear as promising electron deficient receptors for their incorporation as catalysts in anion–π catalysis or as receptors within smart materials and electronics.

Conflicts of interest

There are no conflicts to declare.

Data availability

The data supporting this article have been included as part of the supplementary information (SI). The supplementary information file contains the description of the synthesis and characterizations of the cryptophanes, the chiral stationary phase HPLC reports, the procedures and data for the titration experiments and the DFT calculations. See DOI: https://doi.org/10.1039/d6nj01284A.

Acknowledgements

Y. C. and A. M. thank the Agence Nationale de la Recherche for funding the APICOCAT project, grant ANR-21-CE07-0011 and the Co-LAB project, grant ANR-19-CE07-0024. We would like to thank Antonin Rey for initial experiments, Arnaud Treuvey and the Spectropole in Marseille for characterization. We thank the 'Centre de Calcul Intensif d'Aix-Marseille' for granting us access to its high-performance computing resources.

Notes and references

1 Q. Zhang and K. Tiefenbacher, *Nat. Chem.*, 2015, **7**, 197.
2 P. Restorp and J. Rebek, *J. Am. Chem. Soc.*, 2008, **130**, 11850.
3 D. Fiedler, R. G. Bergman and K. N. Raymond, *Angew. Chem., Int. Ed.*, 2004, **43**, 6748.
4 S. H. A. M. Leenders, R. Gramage-Doria, B. de Bruin and J. N. H. Reek, *Chem. Soc. Rev.*, 2015, **44**, 433.
5 J. M. Lehn, *Acc. Chem. Res.*, 1978, **11**, 49.
6 S. M. Birosa and J. Rebek, *Chem. Soc. Rev.*, 2007, **36**, 93.

7 T. Brotin and J.-P. Dutasta, *Chem. Rev.*, 2009, **109**, 88.
8 D. Zhang, A. Martinez and J.-P. Dutasta, *Chem. Rev.*, 2017, **117**, 4900.
9 O. Perraud, V. Robert, H. Gornitzka, A. Martinez and J.-P. Dutasta, *Angew. Chem., Int. Ed.*, 2012, **51**, 504.
10 C. P. Wren, R. J. Flood, N. M. Mockler, M. Savko, M. Malinska, Q. Shi and P. B. Crowley, *J. Am. Chem. Soc.*, 2025, **147**, 28107.
11 H. A. Fogarty, P. Berthault, T. Brotin, G. Huber, H. Desvaux and J.-P. Dutasta, *J. Am. Chem. Soc.*, 2007, **129**, 10332.
12 M. Zhang, X. Yan, F. Huang, Z. Niu and H. W. Gibson, *Acc. Chem. Res.*, 2014, **47**, 1995.
13 Y. Zhu, M. Tang, H. Zhang, F.-U. Rahman, P. Ballester, J. Rebek Jr., C. A. Hunter and Y. Yu, *J. Am. Chem. Soc.*, 2021, **143**, 12397.
14 O. Taratula, P. A. Hill, N. S. Khan, P. J. Carroll and I. J. Dmochowski, *Nat. Commun.*, 2010, **1**, 148.
15 M. Otte, *Eur. J. Chem.*, 2023, **26**, e202300012.
16 S. C. Bete and M. Otte, *Angew. Chem., Int. Ed.*, 2021, **60**, 18582.
17 A. Platzek, S. Juber, C. Yurtseven, S. Hasegawa, L. Schneider, C. Drechsler, K. E. Ebbert, R. Rudolf, Q.-Q. Yan, J. J. Holstein, L. V. Schäfer and G. H. Clever, *Angew. Chem., Int. Ed.*, 2022, **61**, e202209305.
18 M. Zenka, J. Preinl, E. Pertermann, A. Lützen and K. Tiefenbacher, *Eur. J. Inorg. Chem.*, 2023, e202300110.
19 Y. Zhao, Y. Cotelle, L. Liu, J. López-Andarias, A.-B. Bornhof, M. Akamatsu, N. Sakai and S. Matile, *Acc. Chem. Res.*, 2018, **51**, 2255.
20 Y. Cotelle, V. Lebrun, N. Sakai, T. R. Ward and S. Matile, *ACS Cent. Sci.*, 2016, **2**, 388.
21 Y. Zhao, Y. Cotelle, N. Saka and S. Matile, *J. Am. Chem. Soc.*, 2016, **138**, 4270.
22 M.-S. Yue, N. Luo, X.-D. Wang, Y.-F. Ao, D.-X. Wang and Q.-Q. Wang, *J. Am. Chem. Soc.*, 2025, **147**, 2303.
23 E. Antonetti, Y. Cotelle, A. Martinez and P. Nava, *Phys. Chem. Chem. Phys.*, 2025, **27**, 17997.
24 Q.-H. Ling, J.-L. Zhu, Y. Qin and L. Xu, *Mater. Chem. Front.*, 2020, **4**, 3176.
25 S. Ganta and D. K. Chand, *Inorg. Chem.*, 2018, **57**, 3634.
26 R. Lavendomme, T. K. Ronson and J. R. Nitschke, *J. Am. Chem. Soc.*, 2019, **141**, 12147.
27 Q.-H. Ling, Y. Fu, Z.-C. Lou, B. Yue, C. Guo, X. Hu, W. Lu, L. Hu, W. Wang, M. Zhang, H.-B. Yang and L. Xu, *Adv. Sci.*, 2024, **11**, 2308181.
28 S. P. Black, A. R. Stefankiewicz, M. M. J. Smulders, D. Sattler, C. A. Schalley, J. R. Nitschke and J. K. M. Sanders, *Angew. Chem., Int. Ed.*, 2013, **52**, 5749.
29 S. P. Black, D. M. Wood, F. B. Schwarz, T. K. Ronson, J. J. Holstein, A. R. Stefankiewicz, C. A. Schalley, J. K. M. Sanders and J. R. Nitschke, *Chem. Sci.*, 2016, **7**, 2614.
30 Z. Lu, T. K. Ronson and J. R. Nitschke, *Chem. Sci.*, 2020, **11**, 1097.
31 T. Šolomek, N. E. Powers-Riggs, Y.-L. Wu, R. M. Young, M. D. Krzyaniak, N. E. Horwitz and M. R. Wasielewski, *J. Am. Chem. Soc.*, 2017, **139**, 3348.
32 H.-H. Huang, K. S. Song, A. Prescimone, A. Aster, G. Cohen, R. Mannancherry, E. Vauthey, A. Coskun and T. Šolomek, *Chem. Sci.*, 2021, **12**, 5275.
33 L. Zhang, Y. Jia, F. Meng, L. Sun, F. Cheng, Z. Shi, R. Jiang and X. Song, *J. Alloys Compd.*, 2022, **923**, 166488.
34 S. Fang, E. Li, D. Zhu, G. Wu, Q. Zhang, C. Lin, F. Huang and H. Li, *Chem. Commun.*, 2021, **57**, 6074.
35 D. Shymon, E. Antonetti, S. Chevallier-Michaud, P. Nava, A. Martinez and Y. Cotelle, *Org. Lett.*, 2026, **28**, 1312.
36 L. Miton, E. Antonetti, M. Poujade, J.-P. Dutasta, P. Nava, A. Martinez and Y. Cotelle, *Chem. Commun.*, 2024, **60**, 5217.
37 A. Long, O. Perraud, M. Albalat, V. Robert, J.-P. Dutasta and A. Martinez, *J. Org. Chem.*, 2018, **83**, 6301.
38 F. Peigneguy, C. Oliveras-González, M. Voltz, N. Ibrahim, M. Sallé, N. Avarvari and D. Canevet, *J. Mater. Chem. C*, 2022, **10**, 13989.
39 A. Das and S. Ghosh, *Angew. Chem., Int. Ed.*, 2014, **53**, 1092.

